Reactive and Functional Polymers 203 (2024) 106016

Contents lists available at ScienceDirect

Reactive and Functional Polymers

journal homepage: www.elsevier.com/locate/react

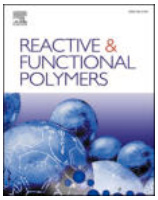

Developing double-crosslinking 3D printed hydrogels for bone tissue engineering

Giuseppe Barberi [a], Sandra Ramos-Díez [b], Calogero Fiorica [a,*], Fabio Salvatore Palumbo [a], Sandra Camarero-Espinosa [b,c], Giovanna Pitarresi [a]

[a] Department of Biological, Chemical and Pharmaceutical Sciences and Technologies (STEBICEF), University of Palermo, via Archirafi 30-32, 90123 Palermo, Italy.
[b] BioSmarTE Lab, POLYMAT, University of Basque Country UPV/EHU, Donostia, /San Sebastián, 20018, Gipuzkoa, Spain.
[c] IKERBASQUE, Basque Foundation for Science, 48009 Bilbao, Spain.

ARTICLE INFO

Keywords:
Double crosslinking
Bone regeneration
3D printing
Injectable hydrogels

ABSTRACT

Bone defects are one of the main causes of disability worldwide. Due to the disadvantages associated with autografts, the latest advances have been focused on tissue regeneration approaches that use injectable hydrogels or 3D printed hydrogel-based structures that could refill appropriately the bone gap area without the need for external fixatives, leading to bone formation in the long term. Injectable hydrogels could be applied in extrusion-based 3D printing as inks; in this sense, double-crosslinking hydrogels appear as ideal candidates. In this work, injectable and printable double crosslinkable hydrogels based on oxidized xanthan gum (XGox) and methacrylate polyaspartylhydrazide (PAHy-MA) were produced. The formation of dynamic hydrazone bonds, occurring between aldehyde groups on the polysaccharide backbone and hydrazine moieties of PAHy-MA, induced an instant gelation, conferring, also, injectability and self-healing properties to the hydrogels. The presence of methacrylic moieties on the synthetic polymer allowed further crosslinking upon UV irradiation that stabilized the hydrogel shape and mitigated its susceptibility to hydrolytic degradation. Obtained hydrogels showed pseudoplastic behaviour and good recovery of viscoelastic properties over time. The physicochemical and rheological characterization highlighted increased stability and higher viscoelastic moduli after photo-crosslinking. The hydrogels also showed good printability, cytocompatibility and the early formation of a bone-like matrix when osteosarcoma-derived cells (MG-63) were cultured in the scaffolds for 21 days, with an increased collagen I deposition, mineralization and the expression of characteristic osteogenic markers.

1. Introduction

Bone defects are currently one of the main causes of morbidity and disability worldwide. [1] Although autografting is considered the gold standard for bone defect repair, it is very limited due to several disadvantages such as the risk of infection, donor-site morbidity and a low integration with host tissues. [2,3] In particular, alveolar and bone defects caused by trauma, extraction or inflammation processes, are difficult to treat with traditional procedures. [4–6] Tissue engineering, has become one of the most used strategies for bone regeneration. [7–10] Among its different approaches, the development of injectable hydrogels, and specifically, polysaccharide-based ones, has received widespread interest and has demonstrated great potential for this purpose. [11–16] Indeed, injectable hydrogels are often used in bone regenerative medicine as a filling material for irregular bone defects that are not subjected to large forces, like alveolar and maxillofacial bone fractures. [5,6,17] Furthermore, the similarity to the soft callus– a cartilage-like intermediate rich in collagen and glycosaminoglycans which is formed during the process of bone regeneration before mineralization– could allow its use as a transient and intermediate structure for the subsequent formation of bone tissue. [14,18,19] There are several strategies in the formulation of injectable hydrogels that exploit physical interactions and/or covalent crosslinking. [20–22] Recently, hydrazone bonds formed by condensation of hydrazine and carbonyl groups have been exploited due to their dynamic nature that can provide a self-healing response to the hydrogels. [23–26] Many researchers have investigated and exploited the advantages of hydrazone bonds for different applications in tissue engineering. Sharma et al. developed an injectable xanthan–poly(ethylene glycol) hydrogel for the controlled release of doxorubicin in 3D cell cultures, exploiting the self-healing

* Corresponding author.
E-mail address: calogero.fiorica@unipa.it (C. Fiorica).

https://doi.org/10.1016/j.reactfunctpolym.2024.106016
Received 2 April 2024; Received in revised form 22 July 2024; Accepted 28 July 2024
Available online 30 July 2024

properties provided by the presence of hydrazone bonds between the two polymers [23].

Xanthan gum is a microbial high molecular weight *exo*-polysaccharide produced by Xanthomonas bacteria, often used in tissue engineering applications due to its high biocompatibility, non-toxicity and non-sensitizing properties. [27,28] The presence of aldehyde groups in xanthan gum, like in other polysaccharides, [29] due to their oxidation, enables their crosslinking with hydrazine groups.

In addition, polyaspartylhydrazides (PAHy) have often been exploited for this purpose. Firstly, synthetized by Giammona G. et al., α,β-polyaspartylhydrazide is a high water-soluble polymer, obtained from a reaction between a polysuccinimide (PSI) and hydrazine. [30] PAHy has been used for a variety of applications (hydrogels and nanoparticles for gene, protein and drug delivery) due to its multiple advantages. Indeed, PAHy is non-toxic, it does not induce any acute immune response, it is synthetized in a facile and affordable manner and it can be functionalized with hydrophilic or hydrophobic moieties due to the reactivity of hydrazine groups. [31–37]

Most of the hydrogels for tissue engineering applications are based on a single-crosslinking network system. However, double-crosslinking network hydrogels offer many advantages. Indeed, combining dynamic and covalent networks, the developed hydrogels usually show not only a self-healing behaviour, but also a good shape retention after injection or extrusion. [26] Dynamic linkages, allow the system to be easily injected and to recover after deformation, while the covalent ones, thanks to their irreversible nature, promote shape retention and improve mechanical and viscoelastic properties. [38–40] In this sense, double-crosslinking hydrogels are good candidates for 3D printing. [38,41] In particular, the reversible dynamic crosslinks are used as the energy dissipation mechanism to improve printability and enhance toughness, while the second irreversible crosslinking can be used to reinforce the structure after printing. [26,39] For this reason, this kind of hydrogels are preferable to the covalently-crosslinked ones because of their easier application on the lesion site and, at the same time, their capability to fill irregular bone defects more accurately, adhering to the edges of the wound and, thus, ensuring greater its permanence in situ. [20,42]

Generally, photo-crosslinkable polymers are used to confer to the system the capability to form covalent irreversible bonds. Acrylate and methacrylate polymers, for example, can rapidly crosslink in the presence of a photoinitiator. [26,43–46] From this point of view, methacrylated gelatin is one of the most exploited photo-crosslinkable biomaterials. [46–51] Shahabipour et al. developed a hydrogel ink based on alginate, gelatin, methacrylated gelatin and hydroxyapatite, exploiting two types of crosslinking, ionotropic (alginate) and covalent, in order to obtain a printable hydrogel and increase its mechanical properties after the printing process. [47]

The aspects highlighted so far would allow the application of double crosslinking or double network hydrogel systems also in 3D printing. [25,38,52–54] Indeed, injectable hydrogels have been often applied in extrusion-based 3D printing as inks. Their printability depends on many aspects, first of all, shear-thinning behaviour and rapid recovery after printing. [47,50] Thus, double-crosslinking hydrogels, appear as ideal candidates. Nevertheless, when a specific application is in view, such as bone regeneration, the presence of factors that stimulate tissue formation is necessary. Hydroxyapatite nanoparticles, account for a composition similar to that of the bone mineral matrix and, thus, have often been used for their osteoinductive activity, [55] incorporated inside hydrogels to improve bone healing, [12,50] showing excellent results.

In this work, we developed injectable double-crosslinking hydrogels as potential inks for bone regeneration. We have designed an injectable hydrogel based on xanthan gum and polyaspartylhydrazide (PAHy) with a dynamic and covalent crosslinking, containing hydroxyapatite nanoparticles. We exploited the hydrazone bond formation between a polysaccharide, an oxidized xanthan gum (XGox), and a polyaminoacid, a polyaspartylhydrazide methacrylate (PAHy-MA). The methacrylic groups on PAHy-MA made it possible to photo-crosslink the system improving the viscoelastic properties. The presence, thus, of both hydrazide and methacrylic groups in the same polymer backbone, allowed to obtain a biomaterial with the capability to make a double-crosslinking (dynamic and covalent). Moreover, the use of a PAHy-MA, thanks to PAHy properties, but also the absence of biomaterial derived from animal sources, could represent a great advantage for the application in bone regenerative medicine.

2. Experimental section

2.1. Materials and methods

Xanthan gum (VANZAN) was purchased by Vanderbilt Minerals LLC. 2-Hydroxy-4′-(2-hydroxyethoxy)-2-methylpropiophenone 98% (photoinitiator, below referred to as PhI), hydroxyapatite nanopowder, N,N-dimetihylformammide (DMF), hydrazine monohydrate, acetone, sodium carbonate anhydrous, sodium hydrogen carbonate >95%, sodium (meta)periodate ($NaIO_4$), ethylene glycol, elastin from bovine neck ligament, oxalic acid, Dulbecco's Phosphate Buffered Saline (DPBS), D_2O, Alizarin Red S have been purchased by Sigma-Aldrich (Italy).

^{1}H NMR spectra were obtained with a Bruker Avance II 400 MHz spectrometer. Samples were prepared by dissolution of 10 mg of samples in 500 μL of Deuterium oxide (D_2O). Data was analysed using Mestrenova software.

FT-IR spectra were recorded with a Bruker Alpha in the wavenumber range of 400 and 4000 cm^{-1}.

Scanning electron microscopy (SEM) analyses of the printed samples were performed by using a TM3030Plus SEM (Hitachi High-Technologies) apparatus; the surface of the samples was previously gold-coated using an SC7620 mini sputter coater/glow discharge system (Quorum).

2.2. Synthesis and characterization of oxidized xanthan gum (XGox)

The oxidation of xanthan gum has been conducted as reported in the literature. [27] Briefly, 500 mg of xanthan gum (XG) were dissolved in Milli Q water at a concentration of 0.6% *w/v* by stirring overnight. Subsequently, an aqueous solution of $NaIO_4$ (0.8% *w/w*) was added dropwise and the reaction was carried out at 40 °C for 3 h in the dark. The molar (X) ratio between the repetitive units of XG and $NaIO_4$ was set at 1:1.5. After 3 h, the reaction was quenched by adding 1.0415 mL of ethylene glycol, which reacted with excess $NaIO_4$. The dispersion was then purified by dialysis (cut-off 12-14 kDa) against Milli Q water for 4 days. The obtained dispersion was then freeze-dried for X days until dry. The product was characterized by FT-IR and ^{1}H NMR analysis.

The oxidation degree (OD) of XGox was calculated as follows by potentiometric titration of the NaOH/hydroxylamine hydrochloride solution: [56].

$$OD = \frac{n\,(NaOH) \times \Delta V}{\frac{m\,(XGox)}{M\,(XGox)}} \times \frac{1}{8} \times 100 \quad (1)$$

where: *n(NaOH)* is 0.1 M, ΔV is the recorded NaOH consumed (L), *m* is the mass of XGox (g), and *M* is the molecular weight of the repeating unit XGox (993 g/mol). The oxidation degree of XGox was calculated to be 25.8% ± 0.2% according to the equation above.

2.3. Synthesis and characterization of methacrylated polyaspartylhydrazide (PAHy-MA)

PAHy-MA was synthesized in two different steps. Firstly a polyaspartylhydrazide (PAHy) was synthesized according to a procedure reported in the literature. [30] Briefly, 4.8 mL of hydrazine monohydrate in 5 mL of DMF were added dropwise and under continuous stirring, to a dispersion solution consisting of 3 g of PSI in 40 mL of DMF.

Table 1
Final composition of formulated hydrogels.

Sample	XGox (%w/v)	PAHy-MA (%w/v)	Hap (%w/v)	PhI (%w/v)
A	1	2	0	0.3
B	1	2	0.01	0.3
C	1	2	0.1	0.3

Photo-crosslinking hydrogels (500 μL) were prepared by irradiating samples for 1 min using a UV Rayonet system with a rotating carousel (365 nm, 100 W).

The reaction temperature was maintained between 24 and 28 °C. After 4 h, during which precipitate formation took place, the reaction mixture was filtered, and the product was washed with acetone until complete removal of the unreacted hydrazine (pH = 7). The obtained product was then vacuum dried, dispersed in Milli Q water to obtain a dispersion with a concentration of 5% and further purified by dialysis against distilled water (cut-off 12-14 kDa). The product was recovered by freeze-drying, with a yield of 94% *w*/w.

In a second step, PAHy-MA was synthesized following reaction conditions reported for the synthesis of methacrylated gelatin with some modifications [51]. Briefly, 500 mg of PAHy were dispersed in 5 mL of carbonate/bicarbonate buffer at pH 9.4 and then 288.66 μL of methacrylic anhydride were added dropwise to the obtained dispersion (molar ratio between methacrylic anhydride and PAHy repetitive units equal to 0.5). The reaction was conducted, under stirring, at 40 °C, in the dark for 1 h, then stopped by the addition of HCl 1 N until a pH = 7.4 was obtained. The dispersion was dialysed against Milli Q water (cut-off 3.5 kDa) and the product was recovered by freeze-drying. The final yield was 70% *w*/w compared to the initial PAHy weight. Finally, the product was characterized by 2,4,6-Trinitrobenzenesulphonic acid (TNBS) assay and ^{1}H NMR analysis.

TNBS assay was performed to calculate the percentage derivation degree (DD %) of PAHy-MA. Briefly, a solution of TNBS (5% *w/v*) (ThermoFisher), diluted in sodium borate buffer (0.1 M, pH = 9.3) 1:5, was added in a ratio of 1:19 to each polymer dispersion (PAHy and PAHy-MA, 25 μg/mL in sodium borate buffer) and incubated for 2 h at 37 °C. Meanwhile, serial dilutions of a tert-Butyl carbazate (TBC) were prepared for the standard curve. Lastly, the absorbance at 492 nm was measured. The DD % of PAHy-MA was calculated with the following equation:

$$DD\% = \left[1 - \frac{n_{NH_2}\ (PAHy - MA)}{n_{NH_2}\ (PAHy)}\right] \times 100 \quad (2)$$

where *n NH$_2$ (PAHy-MA)* and *n NH$_2$ PAHy* are the moles of hydrazine groups of PAHy-MA and PAHy respectively.

2.4. Formulation and characterization of hydrogels

Hydrogels were produced by mixing aqueous solutions of XGox and PAHy-MA. Hydroxyapatite nanoparticles (Hap) and PhI were also dispersed or dissolved in the gelling solution according to the precise weight ratios reported in Table 1.

2.5. Hydrolytic degradation studies

Degradation studies of the materials were performed on freeze-dried hydrogels, prepared as described before (sample A). Scaffolds were accurately weighed (15 mg), immersed in 2 mL of DPBS pH 7.4 and incubated at 37 °C in an orbital shaker. At scheduled times (7, 14, 21 days), samples were repeatedly washed with Milli Q water to remove the DPBS salts, then freeze-dried and re-weighed.

The sample degradation degree was expressed as the percentage of recovered weight percentage (W_r%), calculated by the following equation:

$$W_r\% = \frac{W_f}{W_i} \times 100 \quad (3)$$

where W_f is the weight of the recovered sample (final weight) at each time, and W_i represents the initial weight. Each experiment was performed in triplicate.

2.6. Rheological characterization

The rheological tests were carried out using a DHR-2 TA Instrument rotational rheometer (TA Instruments – Waters S.p.A.) equipped with a flat geometry of 8 mm in diameter with radial groove and a self-heating Peltier plate. Hydrogels were first subjected to a variable amplitude of strain to study storage (G') and loss (G") modules, the linear viscoelastic region (LVR) and the cross point between G' and G" by applying % strain between 0.1% and 5 × 10^3%, under constant temperature (25 °C) and at an angular frequency of 0.5 rad/s. Then, flow sweep experiments were conducted to assess the variation in viscosity at an increasing shear rate from 0.01 s^{-1} to 100.0 s^{-1}, under a constant temperature. To study the recovery and self-healing properties of the samples, recovery time tests were performed by subjecting hydrogels to 7 cycles of 5% and 1.3 × 10^3%, each for 100 s, applying a constant temperature of 25 °C and an angular frequency of 0.5 rad/s. Moreover, frequency sweep tests were carried out at a constant temperature (25 °C), in a range of oscillation frequencies between 0.05 and 50 rad/s, applying a constant % strain of 5.0% (LVR). Lastly, Oscillation time tests were carried out with a strain % of 5%, angular frequency at 0.5 rad/s and temperature at 25 °C for 300 s to evaluate variations of G' and G" over time. Each analysis was carried out on 100 μL of sample. The measurement gap was set to 300 μm for all analyses performed and the excess sample was carefully removed before the start of each experiment. All tests were performed in triplicate.

2.7. 3D printing

A REGEMAT3D Bio V1®bioprinter (3D Regemat, Spain) was used to print porous hydrogel scaffolds of 15 × 15 × 3 mm with a syringe of 5 mL and a 20 GA tip. The samples were printed with pores of 2 × 2 mm and a layer height of 0.30 mm. The infill and flow speed were respectively in the range 5.5–6.5 mm/s and 3.5–4.5 mm/s. The printed structures were photo-crosslinked every two layers under UV light (1000 mW/cm^2 with a curing speed of 1 mm/s). Printability error (P_e) was evaluated using the following formula: [57].

$$Pe = \frac{filament\ diameter\ (d)}{Nozzle\ diameter\ (D)} \quad (4)$$

The measurements were performed using the ImageJ software on SEM images of freeze-dried samples.

2.8. Elastin extraction

The extraction of the water-soluble elastin from elastin of bovine neck (Sigma-Aldrich) was performed as reported in the literature. [46,58] Briefly 5 g of bovine elastin was suspended in 0.25 M oxalic acid solution and hydrolysed by sequential cycles of heating for 1 h in a water boiling bath. The supernatant was collected by centrifugation and the precipitate was treated in the same way until complete hydrolysis. The collected soluble fraction was dialyzed against water using a dialysis membrane tube of 3500 Da cut-off and then freeze-dried.

2.9. Cell culture, scaffold seeding and cytocompatibility tests

An osteoblast cell line, MG-63 (ATCC CRL-1427), was expanded until passage 9 in monolayer culture in α-MEM supplemented with 10% (*v*/v) fetal bovine serum (FBS) at 37 °C with 5% of CO_2 with a cell seeding

density of 5000 cells/cm^2 until 80% confluence. The culture media was changed every 2–3 days.

For cell culture experiments on the scaffolds, XGox was sterilized by UV light (254 nm for 40 min), while PAHy-MA and PhI were sterilized by filtration with a 0.2 μm pore mixed cellulose ester syringe filter prior to printing. After printing, the scaffolds were coated with elastin by covering them with an elastin solution at 500 μg/mL in PBS, followed by 1 h incubation at 37 °C and finally transferred to another plate. Cells at passage 9 were trypsinized, pelleted down by centrifugation at 500 rpm and resuspended to reach a density of 3.0×10^6/mL. 50 μL of the cell suspension were seeded on each scaffold to reach 1.5×10^5 cells/scaffold.

To study the cytocompatibility of the material, scaffolds of 6 × 15 × 3 mm (with pores of 2 × 2 mm) were printed in sterile conditions using a REGEMAT3D Bio V1®bioprinter for the composition A (1% XGox, 2% PAHy-MA, 0.3% PhI, 0% Hap). DNA assay and LDH evaluation were performed on the samples after 24 h and 7 days. All the experiments were performed in triplicate. The total DNA amount was measured with a CyQuant™ cell proliferation assay (Invitrogen), according to the manufacturer's instructions. A value of 6.6×10^{-6} μg of DNA was assumed for each cell to estimate the total cell numbers. At the different time points, the media was removed, and the samples were washed with DPBS two times, then freeze-thawed three times and finally digested with 1 mg/mL Proteinase K (Fisher BioReagents™) in Tris/EDTA buffer at 56 °C overnight. Subsequently, a solution of RNAse A diluted in lysis buffer 1:500 was added in a ratio of 1:1 to each sample and incubated for 1 h at RT. Meanwhile, serial dilutions of a DNA standard were prepared for the standard curve. Lastly, 100 μL of GR-dye solution (diluted 1:200 in lysis buffer) were added to the same volume of each sample in a black bottom microplate, incubated for 15 min at RT and then fluorescence was measured (480 nm excitation, 520 nm emission).

For the LDH, at the different time points, the samples' media was collected and centrifuged at 500 rpm for 10 min to remove any cell, transferred into new tubes and stored at −80 °C until use. LDH content was measured following the manufacturer's instructions. (Cyquant LDH cytotoxicity assay, ThermoFisher).

2.10. Cell differentiation experiment

To evaluate the differentiation of cells seeded on the different scaffolds, samples of 4 × 4 × 3 mm (with a pore of 2 × 2 mm) were printed in sterile conditions for all the compositions A, B, and C. After printing, the scaffolds were coated with the elastin extracted as described previously, and 2.0×10^5 cells were seeded on each scaffold. The scaffolds were incubated in basal medium (α-MEM supplemented with 10% *v*/v FBS) for 24 h and then this was substituted with the differentiation medium (α-MEM supplemented with 10% (*v*/v) FBS, 100 U/mL (1%) penicillin-streptomycin, 200 μM L-ascorbate-2-phohsphate (ASAP), 10 nM dexamethasone and 10 mM β-glycerophosphate). Samples incubated in the basal medium were used as a control. The media was changed every 2–3 days and every week the samples were transferred to new plates. After 14 and 21 days, DNA assay, real-time PCR (RT-PCR), Alizarin Red S assay, immunostaining analyses and SEM were performed.

The following abbreviations were used to refer to the results of these assays: A bm (sample A incubated in basal media), B bm (sample B incubated in basal media), C bm (sample C incubated in basal media), A dm (sample A incubated in differentiation media), B dm (sample B incubated in differentiation media), C dm (sample C incubated in differentiation media).

2.11. Gene expression analysis: RNA isolation and purification, cDNA synthesis and quantitative polymerase chain reaction (qPCR)

After 14 or 21 days of culture in basal and osteogenic media, the seeded scaffolds were rinsed with PBS three times. To lyse the cells, scaffolds were covered with 1 mL of TRIzol for 5 min at RT and freeze-thawed with liquid nitrogen three times. To eliminate proteoglycans of the extracts, which are powerful inhibitors of the Polymerase Chain Reaction, additional centrifugation at 12000 ×*g* for 5 min was done to precipitate them. The supernatant was mixed with 200 μL of $CHCl_3$ shaken vigorously for 15 s and incubated for 3 min at RT, followed by a centrifugation at 12000 ×*g* for 15 min. The upper colourless phase was mixed with 500 μL of isopropanol and incubated for 10 min at RT. After their centrifugation at 12000 ×*g* for 10 min at 4 °C, the RNA formed a gel-like precipitate that was separated and mixed with an equal volume of ethanol. The extracted RNA was purified and eluted following the Invitrogen™ PureLink™ RNA Mini Kit protocol. The concentration of the extracted mRNA solutions was determined using an IMPLEN NanoPhotometer N60/N50 measuring the absorbance of the samples at 260 nm, and their purity grade checking the A260/A280 and A260/A230 absorbance ratios. To carry on the synthesis of complementary DNA, the Applied Biosystems™ High-Capacity RNA-to-cDNA™ Kit manufacturer's instructions were followed on a 20 μL reaction, setting a temperature program of 37 °C for 60 min and 95 °C for 5 min. To perform the qPCR experiment, 10 μL of reverse and forward primer 100 μM solutions were diluted in 980 μL of molecular grade H_2O. 8 μL of primer dilutions (*Col1a1*, *RunX2* and *BGLAP*) were mixed with 2 μL of cDNA solution and 10 μL of SyBR Green 2× in a 96-Well Clear Reaction Plate. A QuantStudio 1 thermocycler (Applied Biosystems) was used with a temperature set-up of a first step with 50 °C for 2 min and 95 °C for 2 min, and then 40 cycles with 95 °C for 15 s and 60 °C for 1 min. The primers used for qPCR experiments are shown in Table 2. C_t values of each sample were determined and employed in the comparative C_T method to calculate the fold change of gene expression in the samples using GAPDH as the housekeeping gene.

Table 2
List of primers used for qPCR experiments.

Gene	Fw (5′-3′)	Rv (5′-3′)
GAPDH	ATG GGG AAG GTG AAG GTC G	TAA AAG CAG CCC TGG TGA CC
Col1a1	AGG GCC AAG ACG AAG ACA TC	AGA TCA CGT CAT CGC ACA ACA
Runx2	AGT GAT TTA GGG CGC ATT CCT	GGA GGG CCG TGG GTT CT
BGLAP	TGA GAG CCC TCA CAC TCC TC	CGC CTG GGT CTC TTC ACT AC

2.12. Alizarin red S staining

For Alizarin Red S (ARS) staining, the samples were firstly fixed with paraformaldehyde (PFA) for 15 min, washed with PBS and then incubated with ARS staining solution (2% w/v) for 1.5 h. The samples were finally washed with Milli Q water and analysed with a Nikon Ts2 light microscope.

2.13. Immunostaining

Samples were fixed with PFA for 15 min and then permeabilized with TritonX-100 0.1% for 15 min followed by washing with PBS. Samples were then blocked with a solution of 3% BSA, 0.01% Triton X-100 in PBS for 1 h and finally washed with a washing buffer (0.3% BSA, 0.001% TritonX-100 in PBS). Afterwards, the samples were stained with Anti-Collagen I Alexa Fluor-488 antibody (Abcam, ab275996, 1:100) for 2 h, washed with WB, stained with Phalloidin Alexa Fluor 568 (Invitrogen, 1:100) for 2 h, washed with Hoechst 33342 (1:500) for 15 min and lastly washed with PBS. The samples were kept in PBS at 4 °C until imaging on a Nikon Eclipse Ti-2 inverted fluorescence microscope.

2.14. Scanning electron microscopy of cell-laden scaffolds

Samples were first fixed with PFA for 15 min and washed with PBS. After fixation, the samples were dehydrated, incubating at room temperature with solutions at higher ethanol concentration in PBS (15 min for each one): 50%, 70%, 80%, 90%, 96% and 100% *v*/v. Then these

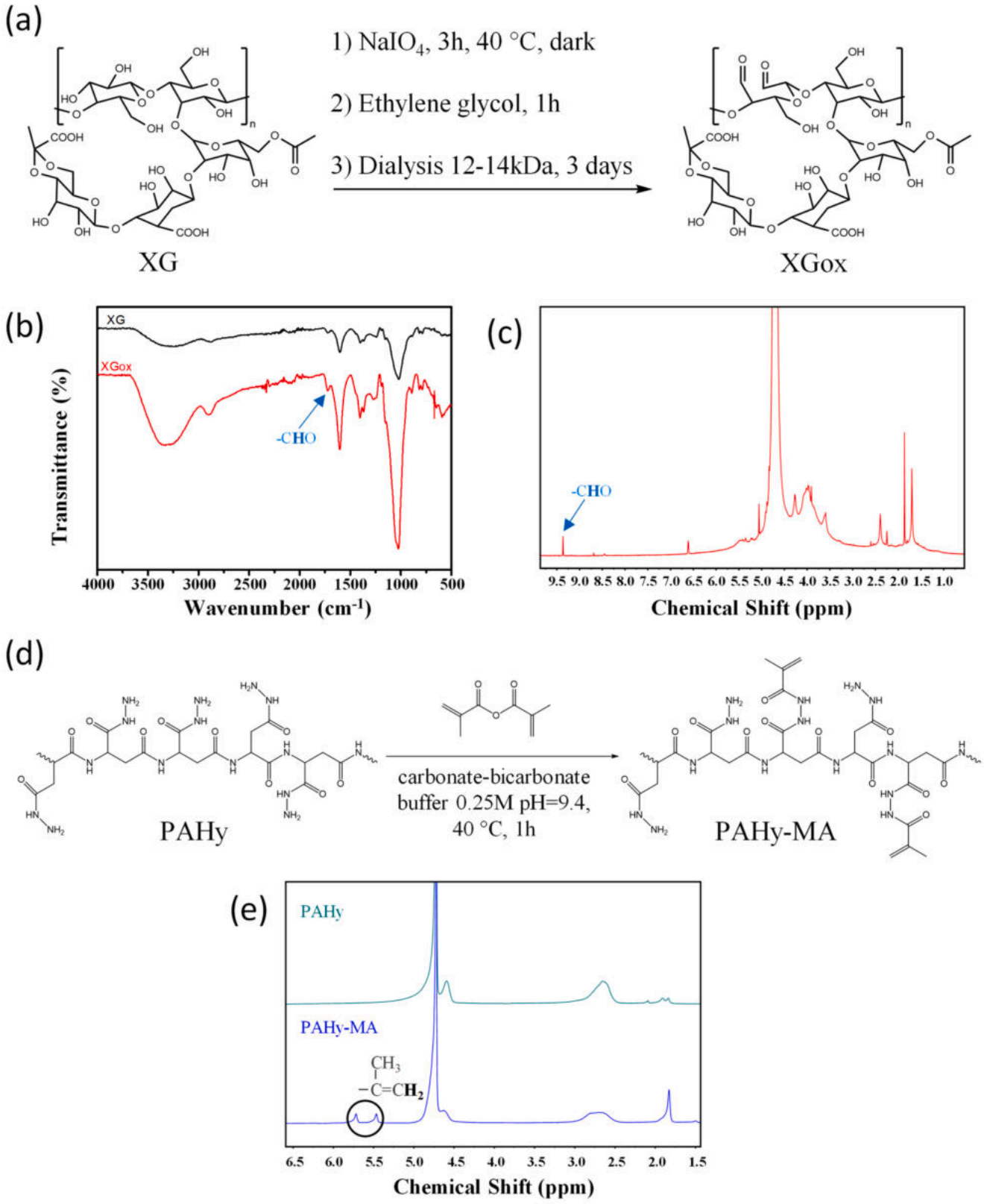

Fig. 1. Schematic representation of XGox synthesis (a). FT-IR spectrum of XG (top, black) and XGox (bottom, red) showing higher intensity of the aldehyde peak at 1723 cm^{-1} in XGox (b). The spectra were normalized to the peak of carbonyl acetate stretching at 1021 cm^{-1}. ^{1}H NMR spectrum of XGox showing the peak associated with the aldehyde at around 9.35 ppm (c). Schematic representation of PAHy-MA synthesis (d). ^{1}H NMR spectra of PAHy (top, green) and PAHy-MA (bottom, blue) showing the appearance of two new peaks at δ 5.4–5.8 ppm, related to the vinyl protons of the methacrylic moieties in PAHy-MA spectra, confirming the functionalization (e). (For interpretation of the references to colour in this figure legend, the reader is referred to the web version of this article.)

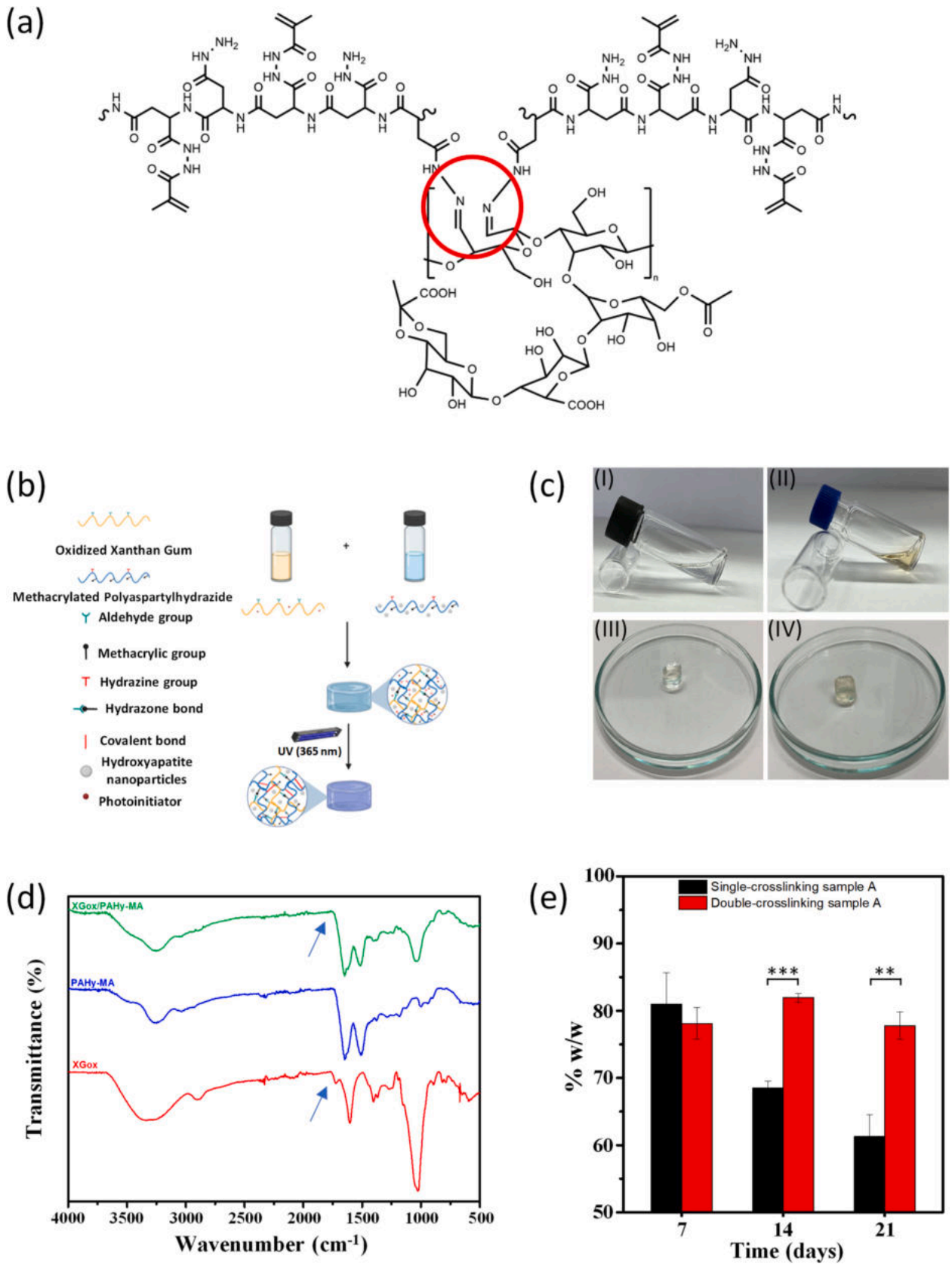

Fig. 2. Schematic representation of hydrazone bond formation in XGox/PAHy-MA hydrogels (a) and of hydrogel A preparation(b). Pictures of XGox dispersion (c, I), PAHy-MA dispersion (c, II), hydrogel A before (c, III) and after (c, IV) the photo-crosslinking process. FT-IR spectra of sample A, PAHy-MA and XGox showing the disappearance of aldehyde peak in XGox/PAHy-MA hydrogel (d). Weight decrease of single-crosslinking and double-crosslinking hydrogels after 7 and 21 days of incubation in PBS (e).

samples were treated with hexamethyldisilazane (50% and 100% v/v in ethanol) and let dry completely overnight with airflow. SEM analyses were performed as described previously (Section 2.1).

2.15. Statistical analysis

All results are reported with a media ± standard deviation and, when applicable the statistical analysis for significance was conducted with the Student's *t*-test, using the function t-test of Microsoft Excel, assuming the not homogenous variance at 2 samples and a dual tile distribution; values with $p < 0.05$ were considered statistically significant (*$p < 0.05$; **$p < 0.01$; ***$p < 0.001$).

3. Results and discussion

3.1. Synthesis and characterization of XGox and PAHy-MA

Dynamic photo-crosslinkable hydrogels with optimal viscoelastic properties, self-healing behaviour and biocompatibility were prepared from XGox and PAHy-MA.

XGox was synthesized through oxidation by sodium (meta)periodate, as reported earlier [27] (Fig. 1a). This kind of reaction allows the formation of ring-opening dialdehyde products through selective cleavage of the C—C bond between the vicinal hydroxyl group of the anhydro-D-glucopyranose residues [59,60]. The reaction was confirmed by FT-IR (Fig. 1b), showing the carbonyl stretching vibration of CHO groups at the 1723 cm^{-1} wavenumber, which was more pronounced in the XGox spectrum as reported elsewhere. [61] The presence of aldehyde groups was also confirmed by ^{1}H NMR (Fig. 1c), through the exhibition of the aldehyde peak at around 9.35 ppm. [62,63]

PAHy-MA was chosen due to the advantages of its forerunner PAHy, which is a water-soluble polymer whose synthesis is easy and inexpensive, its non-toxic character and the absence of acute immune response when administered intradermally to laboratory animals. [30] This led to its widespread use for different applications (hydrogels and nanoparticles for gene, protein and drug delivery). [31–36] Furthermore, the presence of hydrazide moieties allows mixing with aldehyde-functionalized polymers (like oxidized polysaccharides) to form hydrazone-based networks. [23,29]

PAHy was synthesized according to a procedure reported in the literature. [31] The methacrylation reaction was performed in carbonate-bicarbonate buffer (pH = 9.4) with methacrylic anhydride and then the product was purified by dialysis (Fig. 1d). Characterization of PAHy-MA by ^{1}H NMR (Fig. 1e) showed the presence of two peaks at δ 5.4–5.8 ppm, related to vinyl protons of the methacrylic moieties, not found in PAHy ^{1}H NMR spectrum (Fig. 1e, top). The peak at 1.83 ppm is attributable to the methyl of the same functional group. Comparing the area of this peak with that of the peak around 2.5–3 ppm relative to methylene protons of the polyaspartamide chain, the derivation degree in methacrylic groups was approximated to be 36 mol% compared to PAHy repetitive units. This result was confirmed by TNBS assay that showed a derivatization degree of 39 mol%.

3.2. Production and physicochemical characterization of the hydrogels

The hydrogels were formulated by utilizing the formation of hydrazone-based networks (Fig. 2a) and were produced by mixing XGox and PAHy-MA solutions, incorporating hydroxyapatite (Hap) when appropriate (Fig. 2b). In order to evaluate the influence of Hap on the viscoelastic and biological properties of the hydrogels, three different samples were produced with the same amount of XGox (1% *w/v*) and PAHy-MA (2% w/v) and different amounts of Hap (0%, 0.01%, 0.1% w/v) (Table 1).

The gelation process, by mixing the polymer solutions, was very rapid and the hydrogels formed in few seconds. All the obtained hydrogels showed macroscopic differences compared to XGox and PAHy-MA solutions at the same concentration. Indeed, they had a higher viscosity and a gel behaviour as showed by their shape retention capability (Fig. 2c). No macroscopic differences (except the colour) were observed between the hydrogels with and without Hap. Photo-crosslinking caused an increase of stiffness that could be appreciated macroscopically. In this way, double crosslinking systems were obtained: the formation of dynamic hydrazone bonds created a polymer network within the systems, enabling the gelation process after mixing the two polymer solutions. Meanwhile, covalent photo crosslinking through UV irradiation formed another network, which increased the stability in physiological fluids and enhanced the viscoelastic moduli of the resulting systems.

In order to define the optimal viscoelastic properties for 3D printing, other weight ratios XGox:PAHy-MA were tested (1:4, 1:1 and 1:0.5). However, the viscoelastic properties of these samples were too stiff (1:4 XGox:PAHy-MA) or too fluid (1:1 and 1:0.5 XGox:PAHy-MA) to be extruded. Thus, we created hydrogels with a 1:2 XGox:PAHy-MA weight ratio (Fig. 2c) that showed the best combination of fluidity and stiffness for extrusion-based printing. FT-IR analysis confirmed the formation of the hydrazone bond as observed by the disappearance of the aldehyde band at 1723 cm^{-1} (stretching of carbonyl groups), even if it was not possible to appreciate the hydrazone band, as it overlapped with the characteristic bands of PAHy-MA (Fig. 2d). However, the hydrazine moieties could also establish inter-polyelectrolyte interactions with oxidized polysaccharides. Indeed, depending on the pH, they could be protonated and, thus, establish electrostatic interactions with the carboxylate groups of XGox. In turn, these interactions could affect the viscoelastic properties of the hydrogels, but they are not responsible for the gelation process.

To demonstrate that the formation of the hydrogels is due to the hydrazone moieties, non-oxidized xanthan gum was mixed with PAHy-MA (Fig. S1) and no variations in the viscoelastic properties or the gelation process were observed. The presence of hydrazone bonds provides to the system self-healing properties; thus, this approach is often used to develop injectable hydrogels for different applications. However, hydrazide moieties can be further exploited to introduce other functional moieties on PAHy. For example, in this case, the functionalization with methacrylic anhydride gives this biomaterial the capability to undergo photo-crosslinking, allowing it to have in the same backbone two different moieties that provide injectability and hydrolytic stability.

Once the weight ratio of the main components of the hydrogel was established, we tested their stability in physiological fluid (Fig. 2e). Double-crosslinking (covalent and dynamic) and single-crosslinking (dynamic crosslinking) hydrogels showed a different degradation profile over time. While the single-crosslinking hydrogels showed a weight loss that reached 61.29 ± 3.22% of the initial weight over 21 days of the incubation period, the double-crosslinking hydrogels suffered an initial weight loss (to 81,95 ± 0.66%) that remained constant over the next 14 days (77.77% ± 2,05% of the initial weight). This result confirmed the higher stability of the double-crosslinking hydrogels in physiological fluid; their longer degradation time, compared with the single-crosslinking ones, ensures longer stability in the physiological environment. These results suggest that the hydrogel could be injected and photo-crosslinked into the bone defect, allowing a longer permanence of the system in the damaged site.

3.3. Rheological characterization

To evaluate the viscoelastic properties of our crosslinking hydrogels and Hap-containing hydrogels, rheological measurements were performed. Therefore, the analyses carried out, aimed to validate the injectability of the system, and also to verify if it can be used as an ink for 3D printing applications. Usually, hydrogels with a storage modulus in the range of 10^2–10^4 Pa could be considered injectable and with good extrudability. [6,12,64–66] For this reason, we investigated the pseudoplastic behaviour, self-healing properties and the viscoelastic modules

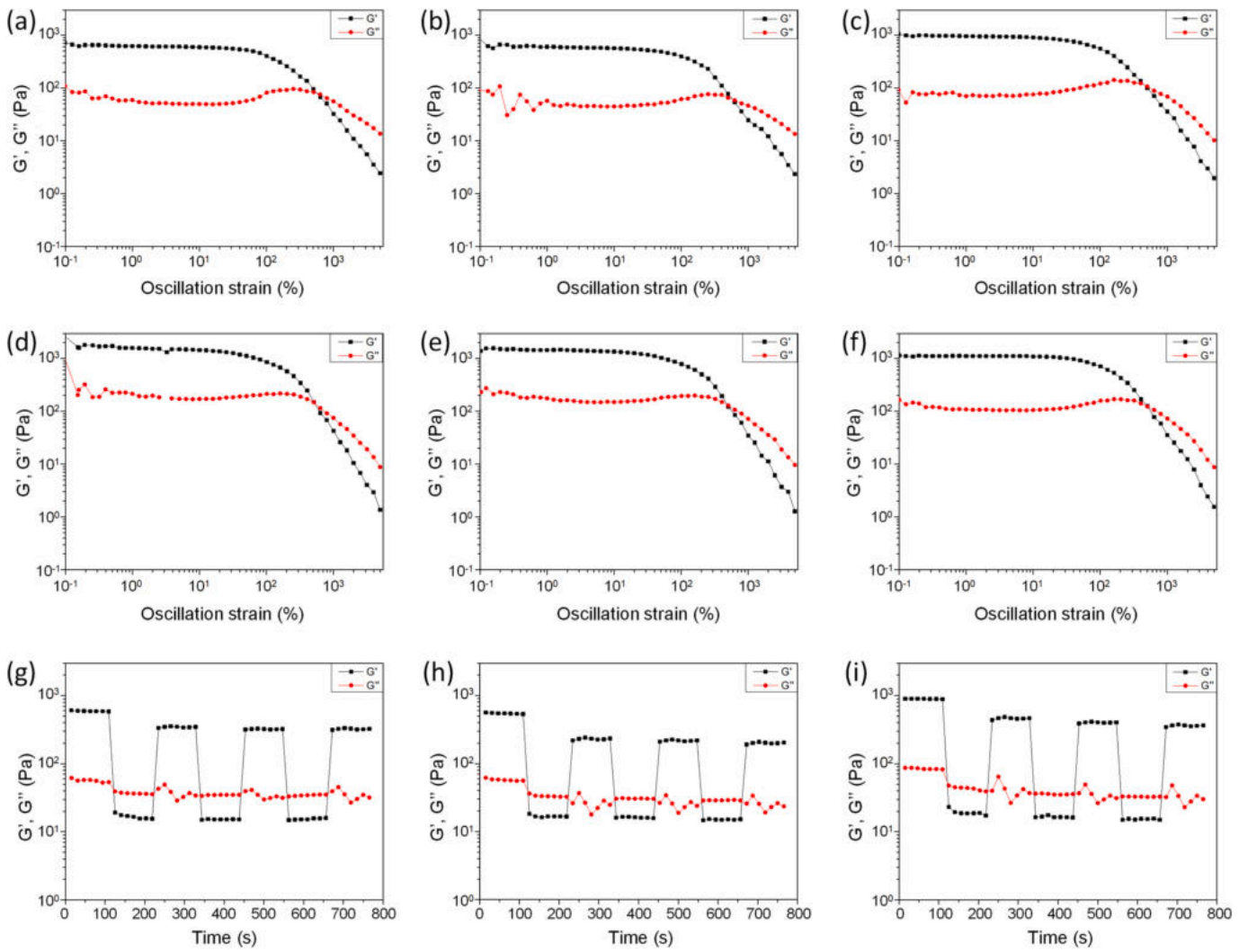

Fig. 3. Storage (G) and loss (G) moduli in function of oscillation strain (a-f) in rheological measurements applying strains % from 0.1% to 5 × 10^3% with an angular frequency of 0.5 rad/s for samples with 0% (sample A), 0.01% (sample B) and 0.1% Hap (sample C) before photo-crosslinking (respectively a, b and c) and after UV irradiation (respectively d, e and f). G´ and G´ as function of time on rheological measurements under alternating strains of 5% and 1.3 × 10^3% with an angular frequency of 0.5 rad/s for samples A (g), B (h) and C (i) before photo-crosslinking.

of the hydrogels with 0, 0.01 and 0.1% Hap.

Storage (G') and loss (G") moduli were initially evaluated with oscillation amplitude analyses (Fig. 3a-c). The results showed that the incorporation of Hap, at the concentration of 0.01% (sample B), does not affect the viscoelastic moduli, which means that the Hap nanoparticles, in this case, do not interfere with the gelation process and with the formation of hydrazine bonds inside the polymer network. Due to their colloidal nature and low concentration, Hap nanoparticles do not increase G' and G". However, by increasing the amount of Hap to 0.1% (sample C) there is a small increase in the viscoelastic moduli before the photo-crosslinking. Moreover, as expected, we observed an increase in the storage modulus after photo-crosslinking (Fig. 3d-f). This is due to the formation of new intermolecular bonds, that leads to the increase of viscoelastic modules. We further evaluated the capability of double-network hydrogels to recover after deformation, as indication of shape retention capability after the extrusion on a 3D printing process. A good recovery of the viscoelastic properties of samples before the photo-crosslinking process was evident (Fig. 3g-i). After the first cycle, G' was about 45%, 60% and 50% of its starting value for samples A, B and C respectively. In the following cycles, the recovery of G' values (referred to the previous cycle) was about 92%, 95% and 90% for samples A, B and C, respectively. This property is due to the dynamic nature of the intermolecular interactions that provide a good recovery of viscoelastic moduli. The self-healing behaviour has also been macroscopically confirmed as shown in Supplementary Information Fig. S2. This allows a 3D printing application of the hydrogel, being able to recover its viscoelastic properties and retain the shape after the extrusion process.

Analysis of the viscosity of the samples under varying shear was carried out on sample A showing a pseudoplastic (or shear-thinning) behaviour (Fig. S3a), with a decreasing viscosity with increasing shear rate. This is probably due to the presence of hydrazone bonds in the polymer network that, due to their dynamic nature, provide to the hydrogel with shear-thinning properties. Oscillation time and frequency sweep tests were carried out on sample A in order to verify the variation of viscoelastic moduli over time and with the increase in frequency. Both the analyses (Supplementary Fig. S3b-c) showed that G' and G" values, measured with a strain % on the linear viscoelastic region (LVR), are independent of time and frequency, suggesting the formation of a stable network structure after the gelation process.

3.4. Printing tests

After rheological characterization, the printability of the inks was evaluated. All the inks were easily extruded through the tip of a printer

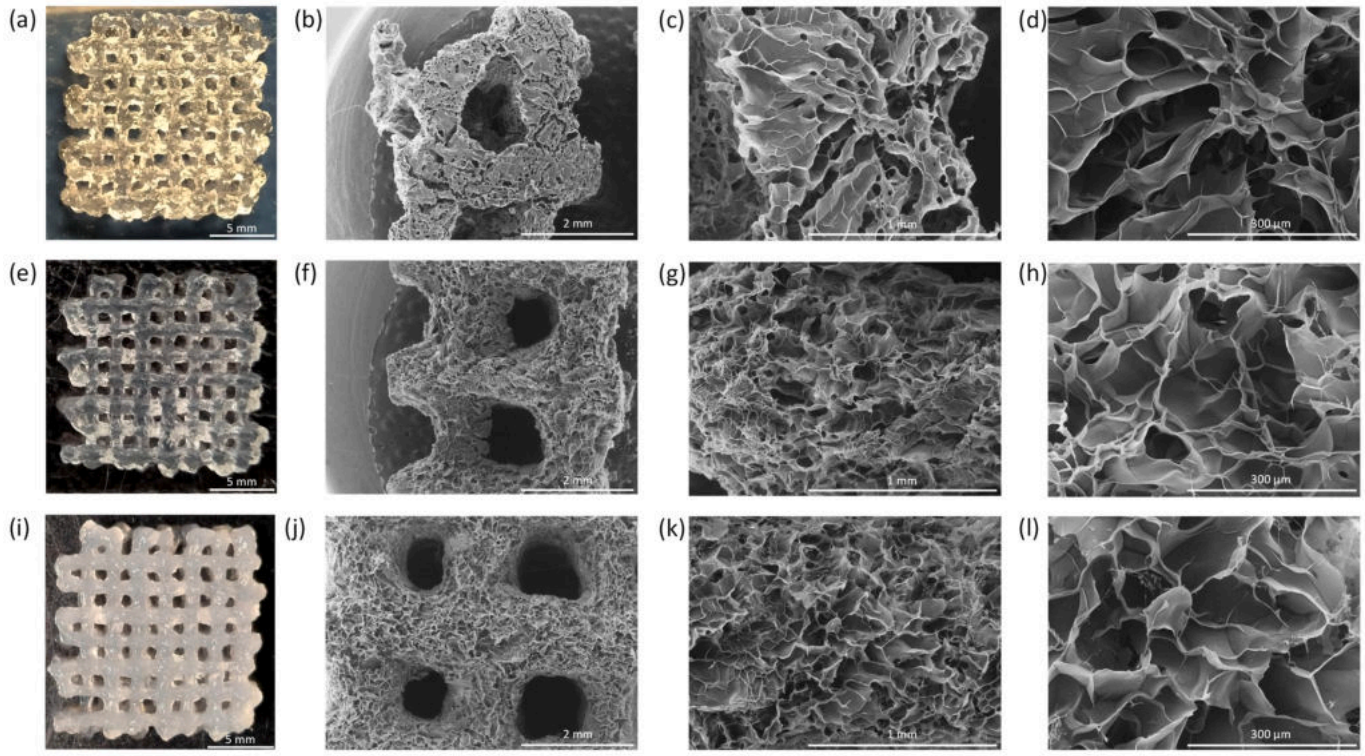

Fig. 4. Printed structures of the different inks and SEM images with different magnifications of the scaffold: sample A (a-d), sample B (e-h) and sample C (i-l).

cartridge, exhibiting shear-thinning properties, as showed by the rheological characterization. More importantly, printed structures of hydrogel composition with 0, 0.01 and 0.1% Hap retained the morphology, especially after the photo-crosslinking process (Fig. 4).

The printability was evaluated on wet and freeze-dried samples. Especially for the wet samples, the printability improved increasing the amount of Hap, according to the reported earlier in the literature. [67,68] The calculated printing error (Pe) was 1.88 ± 0.25, 1.75 ± 0.20 and 1.30 ± 0.008 for samples A (0% Hap), B (0.01% Hap) and C (0.1% Hap), respectively. For the freeze-dried samples a Pe of 1.28 ± 0.17, 1.34 ± 0.12, 1.27 ± 0.07 for samples A (0% Hap), B (0.01% Hap) and C (0.1%) was calculated, respectively. No significant differences could be observed between the samples, although the values could be considered good for all of them and lower than other 3D-printable hydrogels reported in the literature. [57,69]

After evaluating the printability and shape fidelity of the printing process, the printed structures were analysed by SEM (Fig. 4). All the samples showed a porous structure with more defined pores in samples

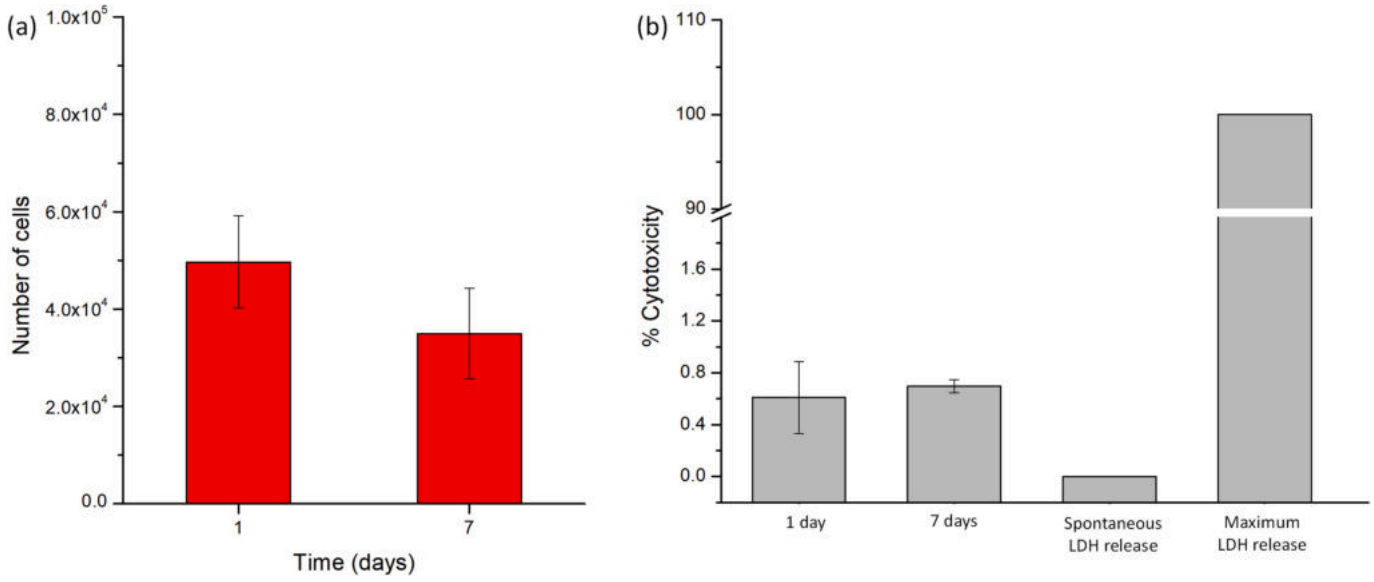

Fig. 5. Number of cells (MG-63) on 3D printed scaffolds of sample A after 24 h and 7 days of culture (a). No significant differences could be observed between the two time points. Cytotoxicity of 3D printed sample A after 24 h and 7 days of culture with MG-63 cells calculated from LDH release measurements (b). Error bars show standard deviation, $n = 3$. No significant differences could be observed between the two time points, although both are significantly different from the positive and negative control.

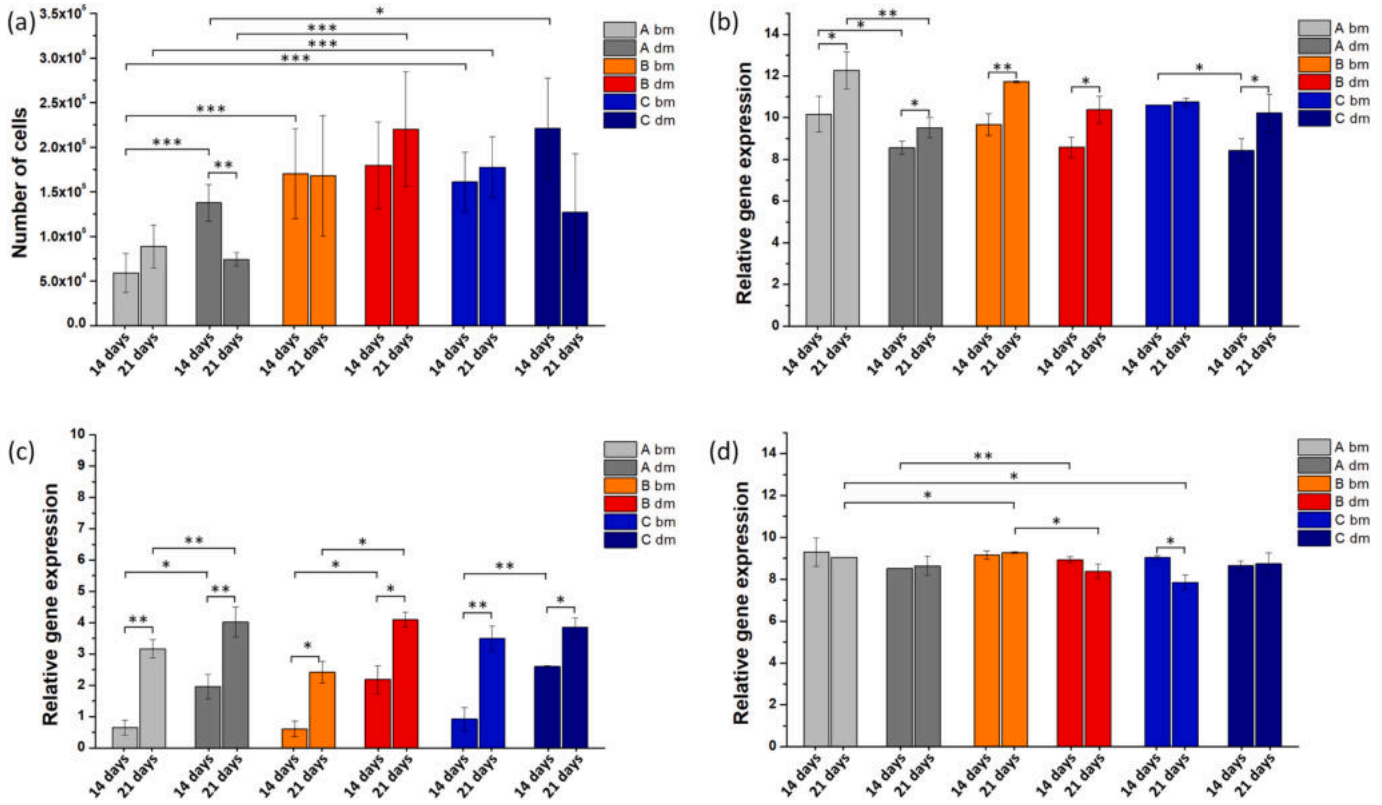

Fig. 6. Number of cells (MG-63) on 3D printed scaffolds of samples A, B and C after 14 and 21 days of culture in differentiation media (dm) or basal media (bm) (a). Relative expression of osteogenic genes BGLAP (b), COL1A1 (c) and RUNX2 (d) by MG-63 cells cultured on 3D printed scaffolds of samples A, B and C and incubated in differentiation media (dm) and basal media (bm) after 14 and 21 days of culture.

with higher concentrations of Hap. The obtained results suggest that double-crosslinking hydrogels, with a shear-thinning and a self-healing behaviour, are promising candidates for 3D printing applications, due to their ease to be injected or extruded and their shape retention and fidelity after the printing process.

3.5. Cytocompatibility tests

To evaluate the applicability of the formulated inks in bone tissue engineering, the cytocompatibility and capability to support cell growth of the biomaterial (XGox/PAHy-MA) was evaluated in vitro with MG-63 cells. After printing, the scaffolds were coated with elastin and then, the cells were seeded on these scaffolds. The elastin coating makes the scaffolds more attractive to cells. Although collagen is the most commonly used protein for this purpose, elastin is frequently reported in the literature for its ability to enhance cell adhesive properties [46,58,70,71]. Additionally, its high-water solubility simplifies the coating process, and the lower cost of the raw material, along with the versatile and reproducible extraction process, further supported this choice.

Regarding the cytocompatibility assays, cells cultured on top of elastin-coated 3D printed structures after 24 h and 7 days of cultures remained viable (Fig. 5a), with a calculated cell number of 49,676,60 ± 9452,67 and 34,982,31 ± 9272,90, respectively (no significant differences). Even if a small number of cells adhered to the surface of the scaffold (maybe because of the small cell density seeded), no reduction of their number over time was detected, indicating the viability of these.

The cytocompatibility of the materials was evaluated through the amount of lactate dehydrogenase (LDH), an enzyme which is present inside the cells that is released when necrosis occurs, released from the cells to the culture medium. After 24 h and 7 days of culture, a cytotoxicity of 0.610 ± 0.278% and 0.698 ± 0.050% was calculated, as compared to spontaneous LDH release controls and lysed cells (Fig. 5b). This result suggests that the materials are cytocompatible and that the system could be applied for tissue engineering applications and the regeneration of bone defects.

3.6. In vitro bone formation potential

To evaluate the capability of the scaffold to promote bone formation, cells were cultured on the 3D printed structures for 14 and 21 days and their proliferation, gene expression and the deposition of bone-specific matrix were evaluated.

Culture of MG-63 cells in basal media on 3D printed scaffolds confirmed their proliferation capability over time (Fig. 6a), with 22,618.25 ± 11,786.12, 25,723.4 ± 12,943.77 and 37,715.04 ± 13,034.81 cells per scaffold in sample A, B and C, respectively, after 24 h of culture and 88,845.90 ± 24,098.52 (A bm), 168,034.38 ± 67,475.62 (B bm), 177,594.42 ± 33,981.58 (C bm), 74,106.44 ± 7599.5 (A dm), 220,110.83 ± 64,312.70 (B dm), 126,895.46 ± 65,974.47 (C dm) after 21 days of culture.

Moreover, samples with Hap (B and C) cultured in basal media showed a significant increase in the number of cells compared to sample A, especially after 14 days (58,960.39 ± 21,672.27 (A bm 14 days), 170,422.48 ± 50,533.75 (B bm 14 days), 160,769.01 ± 33,428.09 (C dm 14 days), 88,845.90 ± 24,098.52 (A bm 21 days), 168,034.38 ± 67,475.62 (B bm 21 days), 177,594.42 ± 33,981.58 (C bm 21 days)). Samples B and C (containing Hap) in differentiation media, however, showed an apparent variation of the cell number (from 14 to 21 days), although not statistically significant (179,731.31 ± 48,729.67 and 220,110.83 ± 64,312.70 (B dm after 14 and 21 days) 220,964.72 ± 56,806.23 and 126,895.46 ± 65,974.47 (C dm 14 and 21 days). This might a result of the activity of the cells, now focused on the differentiation process rather than in proliferation.

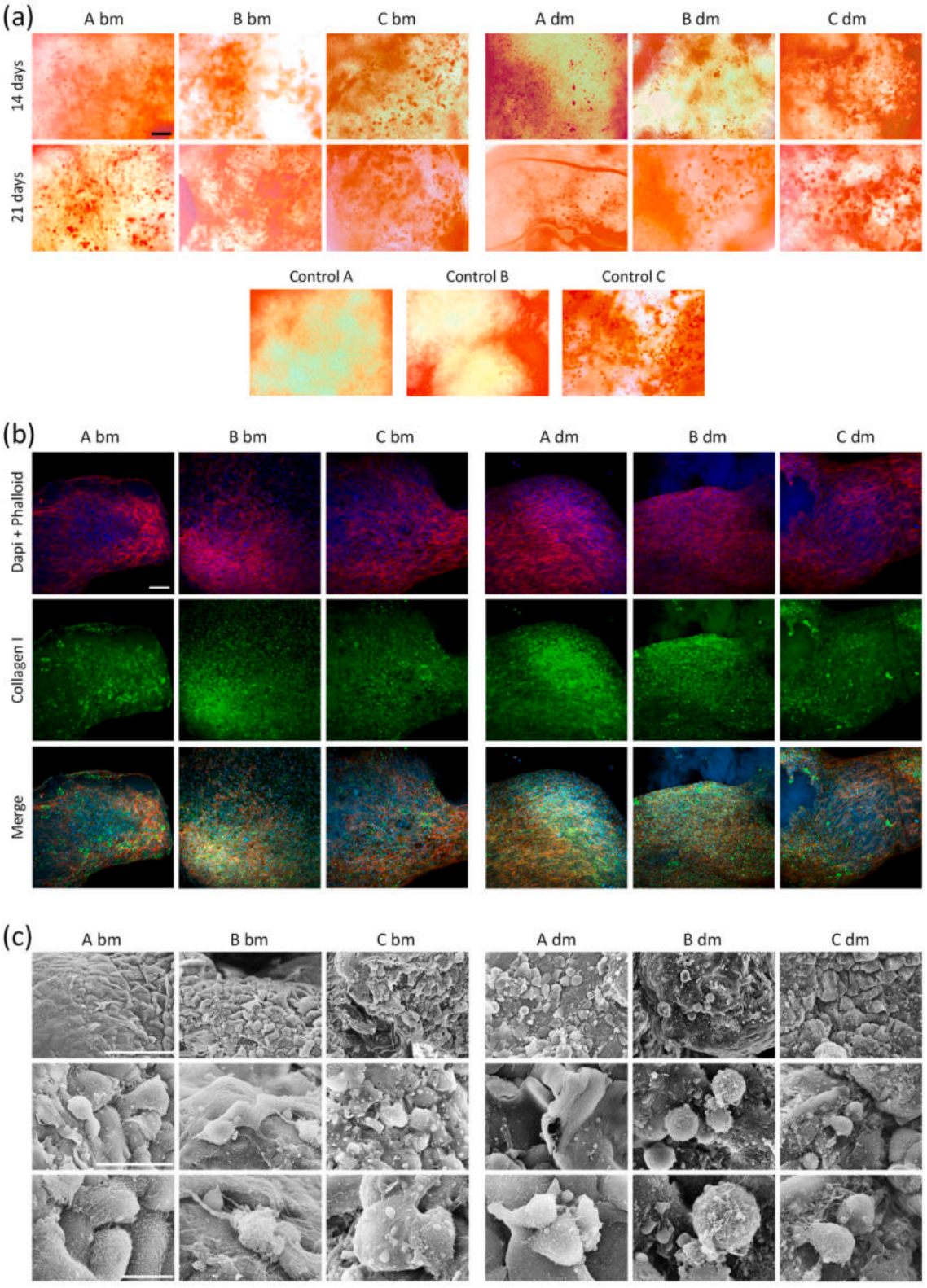

Fig. 7. Mineralization of MG-63 cells cultured on 3D printed scaffolds of samples A, B and C in differentiation media (dm) or basal media (bm) for 21 days visualized in orange-to-red using alizarin red staining assay. Controls A, B and C refer to the samples incubated without cells for 21 days (a). Scale bars are 100 μm. Immunofluorescence images of MG-63 cells cultured on 3D printed scaffolds of samples A, B and C in differentiation (dm) and in basal media (bm) after 21 days of culture (b). Scale bars are 100 μm. SEM images (c) with different magnifications of MG-63 cells cultured on 3D printed scaffolds of samples A, B and C incubated in differentiation media (dm) or basal media (bm) after 21 days of culture. Scale bars are 100 μm (top), 30 μm (middle) and 10 μm (bottom). (For interpretation of the references to colour in this figure legend, the reader is referred to the web version of this article.)

The gene expression of characteristic osteogenic markers osteocalcin (BGLAP), collagen I and RunX2 was evaluated on MG-63 cells after 14 and 21 days of culture on 3D printed scaffolds in basal and differentiation media (Fig. 6b-d). A high relative expression of osteocalcin, a protein solely expressed by osteoblast, was expressed in all samples regardless of the media condition, with no significant differences between the samples with different Hap concentrations (Fig. 6b). Similarly, RunX2, a transcription factor involved in the osteoblastic differentiation process, appeared also highly expressed in cells cultured in all sample types, regardless of the Hap concentration and the culture time (Fig. 6c). In parallel, the genetic expression of collagen I was also significant in all samples, with a higher expression on cells cultured in differentiation media and at the longer culture period of 21 days (Fig. 6d). These data suggest that all sample types, regardless of the Hap concentration, were able to retain an osteoblastic phenotype on seeded MG-63 cells, essential to induce bone formation at later stages.

Once we validated the capability of XGox:PAHy-MA based hydrogels to support cell growth and to retain an osteoblastic phenotype, their capability to induce the deposition of a bone-like matrix was evaluated.

One of the main characteristics of bone formation is the mineralization process. Thus, we evaluated the formation of calcium deposits by Alizarin Red staining (Fig. 7a).

The deposition of calcium was evidenced by the intense red-orange staining that took place on all the scaffolds, regardless of the Hap concentration. As a control, samples of XGox:PAHy-MA with Hap were also analysed, showing a much lower intensity. The formation of a new matrix is more evident in samples A (A dm and A bm) because of the absence of Hap in the starting samples. The alizarin red staining results suggest that the XGox/PAHy-MA scaffolds, promote the deposition of calcium and, hence, the mineralization process essential for bone formation.

Furthermore, the samples were analysed by immunofluorescence techniques to reveal the presence of cells on the scaffolds, the morphology of the cytoskeleton and the production of collagen I (Fig. 7b).

The results show a clear presence of cells on the scaffolds, confirming the DNA assay results. After 14 days of culture, collagen I was visualized in the pericellular space in all sample types in both, basal and differentiation media conditions (Supporting Information Fig. S4). After 21 days of culture, a high deposition of fibrous collagen I is evident in all samples cultured in differentiation media (dm), regardless of the presence of Hap, while in samples cultured in basal media (bm) conditions, collagen I appears to be only pericellular (Fig. 7b). This is in line with the results of COL1A1 gene expression.

SEM images performed on the samples confirmed these results (Fig. 7c and Figure s4b). In particular, the cell density increases from 14 days of culture to 21 days. The mineralization nuclei (visible as bright white dots on the surface of the cells) increase with the amount of Hap in the scaffolds. They are more evident in the sample at 14 days of culture because of the lower cell density on the scaffold surface. Furthermore, it was, also, possible to observe the formation of a fibrous matrix in the samples at both time points, with a more evident deposition in 14-day samples, again, due to lower cell density. Thus, the presence of a fibrous matrix, collagen I deposition and expression as well as mineralization nuclei confirms the in-vitro osteogenesis of the cells seeded on the surface of the scaffolds.

It is evident that, for a complete implementation of the systems, these preliminary results will need to be demonstrated in vivo to confirm both the real osteogenic properties of the scaffolds and their mechanical stability. Moreover, printing tests, considering real shapes of the lesions, need to be carried out for a further application of the systems.

4. Conclusions

In this work, double-crosslinking hydrogels incorporating hydroxyapatite nanoparticles were developed as potential inks for bone regeneration. The hydrogels were formulated using a novel methacrylated polyaspartylhydrazide and an oxidized xanthan gum, exploiting a double-crosslinking: dynamic hydrazone bonds and covalent methacrylic bonds formed upon UV irradiation. The resulting hydrogels demonstrated good stability in physiological fluids (about 22% weight loss after 21 days of incubation) and exhibited interesting rheological properties. Their viscoelastic and shear-thinning behaviour indicated good injectability, while their ability to maintain shape over time suggested good printability, which was confirmed by printing tests. The hydrogels were not cytotoxic and capable of stimulating bone tissue regeneration by increasing the expression of osteogenesis genes, calcium deposition and collagen fibres deposition. These findings suggest that the system could be applied as a potential scaffold for bone tissue engineering both as an injectable hydrogel and by using 3D printing techniques.

CRediT authorship contribution statement

Giuseppe Barberi: Validation, Software, Methodology, Formal analysis, Data curation, Conceptualization, Writing – review & editing, Writing – original draft. **Sandra Ramos-Díez:** Validation, Software, Methodology, Writing – review & editing. **Calogero Fiorica:** Validation, Supervision, Project administration, Conceptualization, Writing – review & editing. **Fabio Salvatore Palumbo:** Validation, Writing – review & editing. **Sandra Camarero-Espinosa:** Validation, Supervision, Project administration, Funding acquisition, Conceptualization. **Giovanna Pitarresi:** Validation, Supervision, Project administration, Funding acquisition, Writing – review & editing.

Declaration of competing interest

The authors declare that they have no known competing financial interests or personal relationships that could have appeared to influence the work reported in this paper.

Data availability

Data will be made available on request.

Acknowledgement

S·C-E acknowledges the Spanish Ministry of Science and Innovation (MINCIN)- State Investigation Agency (AEI) (PID2020-114901RA-I00) and the Basque Government (PIBA_2022_1_0006).

Appendix A. Supplementary data

Supplementary data to this article can be found online at https://doi.org/10.1016/j.reactfunctpolym.2024.106016.

References

[1] K.E. Ensrud, Epidemiology of fracture risk with advancing age, J. Gerontol. A Biol. Sci. Med. Sci. 68 (2013) 1236–1242, https://doi.org/10.1093/GERONA/GLT092.
[2] C.R. Dosier, B.A. Uhrig, N.J. Willett, L. Krishnan, M.T.A. Li, H.Y. Stevens, Z. Schwartz, B.D. Boyan, R.E. Guldberg, Effect of cell origin and timing of delivery for stem cell-based bone tissue engineering using biologically functionalized hydrogels, Tissue Eng. Part A 21 (2015) 156–165, https://doi.org/10.1089/TEN.TEA.2014.0057.
[3] M. Liu, X. Zeng, C. Ma, H. Yi, Z. Ali, X. Mou, S. Li, Y. Deng, N. He, Injectable hydrogels for cartilage and bone tissue engineering, Bone Res. 5 (2017) 1–20, https://doi.org/10.1038/boneres.2017.14.
[4] Y. Ma, Y. Ji, T. Zhong, W. Wan, Q. Yang, A. Li, X. Zhang, M. Lin, Bioprinting-based PDLSC-ECM screening for in vivo repair of alveolar bone defect using cell-laden, injectable and photocrosslinkable hydrogels, ACS Biomater Sci. Eng. 3 (2017) 3534–3545, https://doi.org/10.1021/acsbiomaterials.7b00601.
[5] B. Wang, C. Feng, Y. Liu, F. Mi, J. Dong, Recent advances in biofunctional guided bone regeneration materials for repairing defective alveolar and maxillofacial bone: a review, Jpn. Dent. Sci. Rev. 58 (2022) 233–248, https://doi.org/10.1016/J.JDSR.2022.07.002.

[6] Y. Pan, Y. Zhao, R. Kuang, H. Liu, D. Sun, T. Mao, K. Jiang, X. Yang, N. Watanabe, K.H. Mayo, Q. Lin, J. Li, Injectable hydrogel-loaded nano-hydroxyapatite that improves bone regeneration and alveolar ridge promotion, Mater. Sci. Eng. C 116 (2020) 111158, https://doi.org/10.1016/J.MSEC.2020.111158.
[7] S.S. Lee, X. Du, I. Kim, S.J. Ferguson, Scaffolds for bone-tissue engineering, Matter 5 (2022) 2722–2759, https://doi.org/10.1016/J.MATT.2022.06.003.
[8] N. Amiryaghoubi, M. Fathi, J. Barar, Y. Omidi, Hydrogel-based scaffolds for bone and cartilage tissue engineering and regeneration, React. Funct. Polym. 177 (2022) 105313, https://doi.org/10.1016/J.REACTFUNCTPOLYM.2022.105313.
[9] C. Wang, W. Huang, Y. Zhou, L. He, Z. He, Z. Chen, X. He, S. Tian, J. Liao, B. Lu, Y. Wei, M. Wang, 3D printing of bone tissue engineering scaffolds, Bioact. Mater. 5 (2020) 82–91, https://doi.org/10.1016/J.BIOACTMAT.2020.01.004.
[10] Z. Wang, Y. Wang, J. Yan, K. Zhang, F. Lin, L. Xiang, L. Deng, Z. Guan, W. Cui, H. Zhang, Pharmaceutical electrospinning and 3D printing scaffold design for bone regeneration, Adv. Drug Deliv. Rev. 174 (2021) 504–534, https://doi.org/10.1016/J.ADDR.2021.05.007.
[11] L. Tomasello, C. Fiorica, R. Mauceri, A. Martorana, F.S. Palumbo, G. Pitarresi, G. Pizzolanti, G. Campisi, C. Giordano, G. Cavallaro, Bioactive scaffolds based on amine-functionalized Gellan gum for the osteogenic differentiation of gingival mesenchymal stem cells, ACS Appl. Polym. Mater. 4 (2022) 1805–1815, https://doi.org/10.1021/ACSAPM.1C01586.
[12] G. Pitarresi, F.S. Palumbo, C. Fiorica, F. Bongiovì, A. Martorana, S. Federico, C. M. Chinnici, G. Giammona, Composite hydrogels of alkyl functionalized Gellan gum derivative and hydroxyapatite/Tricalcium phosphate nanoparticles as injectable scaffolds for bone regeneration, Macromol. Biosci. 22 (2022), https://doi.org/10.1002/MABI.202100290, 2100290.
[13] Z. Cao, X. Bai, C. Wang, L. Ren, D. Ma, A simple polysaccharide based injectable hydrogel compositing nano-hydroxyapatite for bone tissue engineering, Mater. Lett. 293 (2021) 129755, https://doi.org/10.1016/J.MATLET.2021.129755.
[14] H. Zhang, S. Wu, W. Chen, Y. Hu, Z. Geng, J. Su, Bone/cartilage targeted hydrogel: strategies and applications, Bioact. Mater. 23 (2023) 156–169, https://doi.org/10.1016/J.BIOACTMAT.2022.10.028.
[15] I. Zia, R. Jolly, S. Mirza, M.S. Umar, M. Owais, M. Shakir, Hydroxyapatite nanoparticles fortified xanthan gum-chitosan based polyelectrolyte complex scaffolds for supporting the Osteo-friendly environment, ACS Appl. Bio Mater. 3 (2020) 7133–7146, https://doi.org/10.1021/ACSABM.0C00948.
[16] X. Wu, Y. Huo, Z. Ci, Y. Wang, W. Xu, B. Bai, J. Hao, G. Hu, M. Yu, W. Ren, Y. Zhang, Y. Hua, G. Zhou, Biomimetic porous hydrogel scaffolds enabled vascular ingrowth and osteogenic differentiation for vascularized tissue-engineered bone regeneration, Appl. Mater. Today 27 (2022) 101478, https://doi.org/10.1016/J.APMT.2022.101478.
[17] X. Bai, M. Gao, S. Syed, J. Zhuang, X. Xu, X.Q. Zhang, Bioactive hydrogels for bone regeneration, Bioact. Mater. 3 (2018) 401–417, https://doi.org/10.1016/J.BIOACTMAT.2018.05.006.
[18] H. Geckil, F. Xu, X. Zhang, S. Moon, U. Demirci, Engineering hydrogels as extracellular matrix mimics, Nanomedicine (London) 5 (2010) 469–484, https://doi.org/10.2217/NNM.10.12.
[19] P.S. Lienemann, M.P. Lutolf, M. Ehrbar, Biomimetic hydrogels for controlled biomolecule delivery to augment bone regeneration, Adv. Drug Deliv. Rev. 64 (2012) 1078–1089, https://doi.org/10.1016/J.ADDR.2012.03.010.
[20] X. Xue, Y. Hu, S. Wang, X. Chen, Y. Jiang, J. Su, Fabrication of physical and chemical crosslinked hydrogels for bone tissue engineering, Bioact. Mater. 12 (2022) 327–339, https://doi.org/10.1016/J.BIOACTMAT.2021.10.029.
[21] G. Biscari, G. Pitarresi, C. Fiorica, D. Schillaci, V. Catania, F. Salvatore Palumbo, G. Giammona, Near-infrared light-responsive and antibacterial injectable hydrogels with antioxidant activity based on a dopamine-functionalized Gellan gum for wound healing, Int. J. Pharm. 627 (2022) 122257, https://doi.org/10.1016/J.IJPHARM.2022.122257.
[22] G. Biscari, Y. Fan, F. Namata, C. Fiorica, M. Malkoch, F.S. Palumbo, G. Pitarresi, Antibacterial broad-Spectrum dendritic/Gellan gum hybrid hydrogels with rapid shape-forming and self-healing for wound healing application, Macromol. Biosci. 23 (2023), https://doi.org/10.1002/MABI.202300224, 2300224.
[23] P.K. Sharma, S. Taneja, Y. Singh, Hydrazone-linkage-based self-healing and injectable xanthan-poly(ethylene glycol) hydrogels for controlled drug release and 3D cell culture, ACS Appl. Mater. Interfaces 10 (2018) 30936–30945, https://doi.org/10.1021/acsami.8b07310.
[24] X. Yang, G. Liu, L. Peng, J. Guo, L. Tao, J. Yuan, C. Chang, Y. Wei, L. Zhang, Highly efficient self-healable and dual responsive cellulose-based hydrogels for controlled release and 3D cell culture, Adv. Funct. Mater. 27 (2017), https://doi.org/10.1002/ADFM.201703174, 1703174.
[25] F.L.C. Morgan, J. Fernández-Pérez, L. Moroni, M.B. Baker, Tuning hydrogels by mixing dynamic cross-linkers: enabling cell-instructive hydrogels and advanced bioinks, Adv. Healthc. Mater. 11 (2022), https://doi.org/10.1002/ADHM.202101576, 2101576.
[26] A.A. Aldana, F.L.C. Morgan, S. Houben, L.M. Pitet, L. Moroni, M.B. Baker, Biomimetic double network hydrogels: combining dynamic and static crosslinks to enable biofabrication and control cell-matrix interactions, J. Polym. Sci. 59 (2021) 2832–2843, https://doi.org/10.1002/POL.20210554.
[27] J. Huang, Y. Deng, J. Ren, G. Chen, G. Wang, F. Wang, X. Wu, Novel in situ forming hydrogel based on xanthan and chitosan re-gelifying in liquids for local drug delivery, Carbohydr. Polym. 186 (2018) 54–63, https://doi.org/10.1016/J.CARBPOL.2018.01.025.
[28] A. Kumar, K.M. Rao, S.S. Han, Application of xanthan gum as polysaccharide in tissue engineering: a review, Carbohydr. Polym. 180 (2018) 128–144, https://doi.org/10.1016/J.CARBPOL.2017.10.009.
[29] T. Wu, C. Cui, Y. Huang, Y. Liu, C. Fan, X. Han, Y. Yang, Z. Xu, B. Liu, G. Fan, W. Liu, Coadministration of an adhesive conductive hydrogel patch and an injectable hydrogel to treat myocardial infarction, ACS Appl. Mater. Interfaces 12 (2020) 2039–2048, https://doi.org/10.1021/acsami.9b17907.
[30] G. Giammona, B. Carlisi, G. Cavallaro, G. Pitarresi, S. Spampinato, A new water-soluble synthetic polymer, α,β-polyasparthydrazide, as potential plasma expander and drug carrier, J. Control. Release 29 (1994) 63–72, https://doi.org/10.1016/0168-3659(94)90122-8.
[31] R.S. Wu, J. Lin, Y.M. Xing, Z.L. Dai, L.W. Wang, X.P. Zhang, pH-sensitive black phosphorous–incorporated hydrogel as novel implant for cancer treatment, J. Pharm. Sci. 108 (2019) 2542–2551, https://doi.org/10.1016/J.XPHS.2019.03.003.
[32] K. Yang, X. Zhao, W. Wei, C.X. Lin, L. Sun, Z. Wei, Q. Huang, X. Ge, M. Zrínyi, Y. M. Chen, A novel injectable and self-biodegradable poly(aspartic acid) hydrogel, Mater. Des. 226 (2023) 111662, https://doi.org/10.1016/J.MATDES.2023.111662.
[33] G. Pitarresi, G. Cavallaro, G. Giammona, G. De Guidi, M.G. Salemi, S. Sortino, New hydrogel matrices containing an anti-inflammatory agent. Evaluation of in vitro release and photoprotective activity, Biomaterials 23 (2002) 537–550, https://doi.org/10.1016/S0142-9612(01)00136-3.
[34] G. Giammona, G. Cavallaro, L. Maniscalco, E.F. Craparo, G. Pitarresi, Synthesis and characterisation of novel chemical conjugates based on α,β-polyaspartylhydrazide and β-cyclodextrins, Eur. Polym. J. 42 (2006) 2715–2729, https://doi.org/10.1016/J.EURPOLYMJ.2006.05.005.
[35] M. Licciardi, G. Cavallaro, M. Di Stefano, G. Pitarresi, C. Fiorica, G. Giammona, New self-assembling polyaspartylhydrazide copolymer micelles for anticancer drug delivery, Int. J. Pharm. 396 (2010) 219–228, https://doi.org/10.1016/J.IJPHARM.2010.06.021.
[36] E. Pedone, G. Cavallaro, S.C.W. Richardson, R. Duncan, G. Giammona, α,β-poly (asparthylhydrazide)–glycidyltrimethylammonium chloride copolymers (PAHy–GTA): novel polymers with potential for DNA delivery, J. Control. Release 77 (2001) 139–153, https://doi.org/10.1016/S0168-3659(01)00459-X.
[37] R. Zhang, Z. Huang, M. Xue, J. Yang, T. Tan, Detailed characterization of an injectable hyaluronic acid-polyaspartylhydrazide hydrogel for protein delivery, Carbohydr. Polym. 85 (2011) 717–725, https://doi.org/10.1016/J.CARBPOL.2011.02.014.
[38] F.L.C. Morgan, L. Moroni, M.B. Baker, Dynamic bioinks to advance bioprinting, Adv. Healthc. Mater. 9 (2020), https://doi.org/10.1002/ADHM.201901798, 1901798.
[39] Z. Gu, K. Huang, Y. Luo, L. Zhang, T. Kuang, Z. Chen, G. Liao, Double network hydrogel for tissue engineering, Wiley Interdiscip. Rev. Nanomed. Nanobiotechnol. 10 (2018) e1520, https://doi.org/10.1002/WNAN.1520.
[40] A.A. Aldana, S. Houben, L. Moroni, M.B. Baker, L.M. Pitet, Trends in double networks as bioprintable and injectable hydrogel scaffolds for tissue regeneration, ACS Biomater Sci. Eng. 7 (2021) 4077–4101, https://doi.org/10.1021/acsbiomaterials.0c01749.
[41] C. Mota, S. Camarero-Espinosa, M.B. Baker, P. Wieringa, L. Moroni, Bioprinting: from tissue and organ development to in vitro models, Chem. Rev. 120 (2020) 10547–10607, https://doi.org/10.1021/acs.chemrev.9b00789.
[42] Y. Gao, K. Peng, S. Mitragotri, Covalently crosslinked hydrogels via step-growth reactions: crosslinking chemistries, polymers, and clinical impact, Adv. Mater. 33 (2021), https://doi.org/10.1002/ADMA.202006362, 2006362.
[43] S. Maiz-Fernández, L. Pérez-Álvarez, U. Silván, J.L. Vilas-Vilela, S. Lanceros-Mendez, Photocrosslinkable and self-healable hydrogels of chitosan and hyaluronic acid, Int. J. Biol. Macromol. 216 (2022) 291–302, https://doi.org/10.1016/J.IJBIOMAC.2022.07.004.
[44] C.A. Vilela, C. Correia, A. da Silva Morais, T.C. Santos, A.C. Gertrudes, E. S. Moreira, A.M. Frias, D.A. Learmonth, P. Oliveira, J.M. Oliveira, R.A. Sousa, J. D. Espregueira-Mendes, R.L. Reis, In vitro and in vivo performance of methacrylated gellan gum hydrogel formulations for cartilage repair*, J. Biomed. Mater. Res. Part A. 106 (2018) 1987–1996, https://doi.org/10.1002/JBM.A.36406.
[45] K.T. Nguyen, J.L. West, Photopolymerizable hydrogels for tissue engineering applications, Biomaterials 23 (2002) 4307–4314, https://doi.org/10.1016/S0142-9612(02)00175-8.
[46] D.M. Tian, H.H. Wan, J.R. Chen, Y. Bin Ye, Y. He, Y. Liu, L.Y. Tang, Z.Y. He, K. Z. Liu, C.J. Gao, S.L. Li, Q. Xu, Z. Yang, C. Lai, X.J. Xu, C.S. Ruan, Y.S. Xu, C. Zhang, L. Luo, L.P. Yan, In-situ formed elastin-based hydrogels enhance wound healing via promoting innate immune cells recruitment and angiogenesis, Mater. Today Bio. 15 (2022) 100300, https://doi.org/10.1016/J.MTBIO.2022.100300.
[47] F. Shahabipour, M. Tavafoghi, G.E. Aninwene, S. Bonakdar, R.K. Oskuee, M. A. Shokrgozar, T. Potyondy, F. Alambeigi, S. Ahadian, Coaxial 3D bioprinting of tri-polymer scaffolds to improve the osteogenic and vasculogenic potential of cells in co-culture models, J. Biomed. Mater. Res. Part A 110 (2022) 1077–1089, https://doi.org/10.1002/JBM.A.37354.
[48] W. Schuurman, P.A. Levett, M.W. Pot, V. Weeren, W.J.A. Dhert, D.W. Hutmacher, F.P.W. Melchels, T.J. Klein, J. Malda, Gelatin-methacrylamide hydrogels as potential biomaterials for fabrication of tissue-engineered cartilage constructs, Macromol. Biosci. 13 (2013) 551–561, https://doi.org/10.1002/mabi.201200471.
[49] Y. Wang, Y. Chen, J. Zheng, L. Liu, Q. Zhang, Three-dimensional printing self-healing dynamic/photocrosslinking gelatin-hyaluronic acid double-network hydrogel for tissue engineering, ACS Omega 7 (2022) 12076–12088, https://doi.org/10.1021/ACSOMEGA.2C00335.
[50] A.R. Osi, H. Zhang, J. Chen, Y. Zhou, R. Wang, J. Fu, P. Müller-Buschbaum, Q. Zhong, Three-dimensional-printable thermo/photo-cross-linked methacrylated

chitosan-gelatin hydrogel composites for tissue engineering, ACS Appl. Mater. Interfaces 13 (2021) 22902–22913, https://doi.org/10.1021/ACSAMI.1C01321.
[51] M. Zhu, Y. Wang, G. Ferracci, J. Zheng, N.J. Cho, B.H. Lee, Gelatin methacryloyl and its hydrogels with an exceptional degree of controllability and batch-to-batch consistency, Sci. Rep. 91 (9) (2019) 1–13, https://doi.org/10.1038/s41598-019-42186-x.
[52] T. Zhang, W. Zhao, Z. Xiahou, X. Wang, K. Zhang, J. Yin, Bioink design for extrusion-based bioprinting, Appl. Mater. Today 25 (2021) 101227, https://doi.org/10.1016/J.APMT.2021.101227.
[53] G. Pitarresi, A. Martorana, F.S. Palumbo, C. Fiorica, G. Giammona, New gellan gum-graft-poly(D,L-lactide-co-glycolide) copolymers as promising bioinks: synthesis and characterization, Int. J. Biol. Macromol. 162 (2020) 1653–1667, https://doi.org/10.1016/j.ijbiomac.2020.07.254.
[54] A. Martorana, G. Pitarresi, F.S. Palumbo, G. Barberi, C. Fiorica, G. Giammona, Correlating rheological properties of a Gellan gum-based bioink: a study of the impact of cell density, Polymers (Basel) 14 (2022), https://doi.org/10.3390/POLYM14091844.
[55] A. Martorana, C. Fiorica, F.S. Palumbo, S. Federico, G. Giammona, G. Pitarresi, Redox responsive 3D-printed nanocomposite polyurethane-urea scaffold for doxorubicin local delivery, J. Drug Deliv. Sci. Technol. 88 (2023) 104890, https://doi.org/10.1016/J.JDDST.2023.104890.
[56] J. Guo, L. Ge, X. Li, C. Mu, D. Li, Periodate oxidation of xanthan gum and its crosslinking effects on gelatin-based edible films, Food Hydrocoll. 39 (2014) 243–250, https://doi.org/10.1016/J.FOODHYD.2014.01.026.
[57] D.K. Patel, T.V. Patil, K. Ganguly, S.D. Dutta, K.T. Lim, Nanocellulose-assisted 3D-printable, transparent, bio-adhesive, conductive, and biocompatible hydrogels as sensors and moist electric generators, Carbohydr. Polym. 315 (2023) 120963, https://doi.org/10.1016/J.CARBPOL.2023.120963.
[58] F.S. Palumbo, G. Pitarresi, C. Fiorica, S. Rigogliuso, G. Ghersi, G. Giammona, Chemical hydrogels based on a hyaluronic acid-graft-α-elastin derivative as potential scaffolds for tissue engineering, Mater. Sci. Eng. C 33 (2013) 2541–2549, https://doi.org/10.1016/J.MSEC.2013.02.015.
[59] W. Wang, M.Y. Liu, M. Shafiq, H.Y. Li, R. Hashim, M. El-Newehy, H. El-Hamshary, Y. Morsi, X. Mo, Synthesis of oxidized sodium alginate and its electrospun bio-hybrids with zinc oxide nanoparticles to promote wound healing, Int. J. Biol. Macromol. 232 (2023) 123480, https://doi.org/10.1016/J.IJBIOMAC.2023.123480.
[60] S. Das, G. Dalei, In situ forming dialdehyde xanthan gum-gelatin Schiff-base hydrogels as potent controlled release fertilizers, Sci. Total Environ. 875 (2023) 162660, https://doi.org/10.1016/J.SCITOTENV.2023.162660.
[61] F.A. Ngwabebhoh, O. Zandraa, R. Patwa, N. Saha, Z. Capáková, P. Saha, Self-crosslinked chitosan/dialdehyde xanthan gum blended hypromellose hydrogel for the controlled delivery of ampicillin, minocycline and rifampicin, Int. J. Biol. Macromol. 167 (2021) 1468–1478, https://doi.org/10.1016/J.IJBIOMAC.2020.11.100.
[62] M. Hu, X. Peng, S. Shi, C. Wan, C. Cheng, X. Yu, Dialdehyde xanthan gum and curcumin synergistically crosslinked bioprosthetic valve leaflets with anti-thrombotic, anti-inflammatory and anti-calcification properties, Carbohydr. Polym. 310 (2023) 120724, https://doi.org/10.1016/J.CARBPOL.2023.120724.
[63] D. Paiva, C. Gonçalves, I. Vale, M.M.S.M. Bastos, F.D. Magalhães, Oxidized xanthan gum and chitosan as natural adhesives for Cork, Polymers (Basel) 8 (2016), https://doi.org/10.3390/POLYM8070259.
[64] S.D. Dutta, K. Ganguly, A. Randhawa, T.V. Patil, D.K. Patel, K.T. Lim, Electrically stimulated 3D bioprinting of gelatin-polypyrrole hydrogel with dynamic semi-IPN network induces osteogenesis via collective signaling and immunopolarization, Biomaterials 294 (2023) 121999, https://doi.org/10.1016/J.BIOMATERIALS.2023.121999.
[65] X. Liu, Y. Zhang, Z. Hussain, P. Zheng, M. Xu, H. Zhao, Y. Liu, Y. Cao, I. Ullah, A. Osaka, R. Pei, Self-biomineralized in situ injectable CaSO4 nanorods-enriched collagen-hyaluronic acid composite hydrogels for biomimetic bone reconstruction in a minimally invasive manner, Appl. Mater. Today 30 (2023) 101693, https://doi.org/10.1016/J.APMT.2022.101693.
[66] W. Ma, M. Yang, C. Wu, S. Wang, M. Du, Bioinspired self-healing injectable nanocomposite hydrogels based on oxidized dextran and gelatin for growth-factor-free bone regeneration, Int. J. Biol. Macromol. 251 (2023) 126145, https://doi.org/10.1016/J.IJBIOMAC.2023.126145.
[67] E. Ojeda, Á. García-Barrientos, N. Martínez de Cestafe, J.M. Alonso, R. Pérez-González, V. Sáez-Martínez, Nanometric hydroxyapatite particles as active ingredient for bioinks: a review, Macromol 2 (2022) 20–29, https://doi.org/10.3390/MACROMOL2010002.
[68] P. Comeau, T. Willett, Printability of methacrylated gelatin upon inclusion of a chloride salt and hydroxyapatite nano-particles, Macromol. Mater. Eng. 304 (2019), https://doi.org/10.1002/MAME.201900142, 1900142.
[69] S.D. Dutta, J. Hexiu, D.K. Patel, K. Ganguly, K.T. Lim, 3D-printed bioactive and biodegradable hydrogel scaffolds of alginate/gelatin/cellulose nanocrystals for tissue engineering, Int. J. Biol. Macromol. 167 (2021) 644–658, https://doi.org/10.1016/J.IJBIOMAC.2020.12.011.
[70] X. Wang, Z. Bai, K. Li, J. Dong, H. Zhang, X. Liu, W. Han, Q. Li, Bioinspired PLCL/elastin nanofibrous vascular tissue engineering scaffold enhances endothelial cells and inhibits smooth muscle cells, Biomacromolecules 24 (2023) 2741–2754, https://doi.org/10.1021/ACS.BIOMAC.3C00175/ASSET/IMAGES/LARGE/BM3C00175_0012.JPEG.
[71] C. Fiorica, F.S. Palumbo, G. Pitarresi, M. Allegra, R. Puleio, G. Giammona, Hyaluronic acid and α-elastin based hydrogel for three dimensional culture of vascular endothelial cells, J. Drug Deliv. Sci. Technol. 46 (2018) 28–33, https://doi.org/10.1016/J.JDDST.2018.04.017.